# Mapping the parameters of prion-induced neuropathology

**Michael P. H. Stumpf*† and David C. Krakauer‡**

*The Wellcome Trust Centre for the Epidemiology of Infectious Disease, Department of Zoology, South Parks Road, Oxford OX1 3PS, United Kingdom; and ‡Institute for Advanced Study, Princeton, NJ 08540

Communicated by Robert May, University of Oxford, Oxford, United Kingdom, July 7, 2000 (received for review December 20, 1999)

**We present a theoretical framework that enables us to dissect out the parametric dependencies of the pathogenesis of prion diseases. We are able to determine the influence of both host-dependent factors (connectivity, cell density, protein synthesis rate, and cell death) and strain-dependent factors (cell tropism, virulence, and replication rate). We use a model based on a linked system of differential equations on a lattice to explore how the regional distribution of central nervous system pathology in Creutzfeldt-Jakob disease, Gerstmann-Sträussler-Scheinker syndrome, and fatal familial insomnia relates to each of these factors. The model then is used to make qualitative predictions about the pathology for two possible hypothetical triggers of neuronal loss in prion diseases. Pathological progression in overexpressing mouse models has been shown to depend on the site of initial infection. The model allows us to compare the pathologies resulting from different inoculation routes.**

strain | transmissible spongiform encephalopathies

Transmissible spongiform encephalopathies are neurodegenerative disorders characterized by an accumulation of a protease-resistant isoform ($PrP^{Sc}$) of the cellular prion protein ($PrP^{c}$) (1, 2). The presence of $PrP^{Sc}$ within nervous tissue results in the formation of amyloid plaques, spongiform changes, reactive astrocytosis, and neuronal loss (3–5). A characteristic feature of these diseases is the large degree of variation in the distribution and magnitude of pathological changes associated both with the host species and the $PrP^{Sc}$ strain (6, 7). These variations have been attributed to several factors including the kinetics of prion propagation, cell tropism, differential toxicity, and host neuro-anatomy and genetic makeup. In experimental systems it is difficult to separate these diverse causes and thereby determine the impact of each variable independently. In the present study we develop a model for prion propagation within the central nervous system, which allows us to explore each of the parameters involved in prion pathogenesis.

All of the known prion diseases in animals and humans can be correlated with an accumulation of $PrP^{Sc}$ in the central nervous system, suggesting that the information carrying pathogen is a protein (8). Pronounced differences in human pathology emerge in comparisons of Creutzfeldt-Jakob disease (CJD), Gerstmann-Sträussler-Scheinker syndrome (GSS), and fatal familial insomnia (FFI) cases (3–5, 9). In familial CJD, loss of neurons and astrocytosis is prominent in gray matter, and PrP amyloid plaques sometimes are reported. These plaques tend to be found in the cerebellum adjacent to the Purkinje cells and sometimes are arranged in arrays. In new variant CJD numerous kuru-type PrP plaques are observed surrounded by a halo of spongiform degeneration. The number of plaques in CJD correlates positively with disease latency. In iatrogenic CJD, lesions and plaques are distributed more diffusely throughout the brain (3). In kuru around 70% of cases have plaques, and the number is greater in long latency cases. In GSS PrP plaques are common and have a unique multicentric configuration; in FFI no plaques have been observed. A similar spectrum of pathology is observed in the animal prion diseases (14). The genotype of the host has an enormous influence on disease susceptibility and progression. For example, mutations at codon 129 of the human prion gene have been shown to be as important in determining pathology as the PrP isotype (11).

## Methods

This paper differs from previous theoretical work on prion infection (12–16) as it focuses on pathogenesis in the brain. This approach allows us to explore mechanisms giving rise to variations in the neuropathology. We start with a description of $PrP^{Sc}$ replication kinetics. Throughout we assume that $PrP^{Sc}$ is required for the transformation of $PrP^{c}$, thus we subscribe to a protein-only transmission mechanism. This mechanism has been suggested to involve either some form of nucleation-dependent aggregation (15) or a conformational change of the PrP (1). In both cases one describes the metabolic pathways by which the diseased form of the protein is formed from the healthy $PrP^{c}$ and how it is then incorporated into $\beta$-amyloid. We model this process qualitatively and use a generic realization of the metabolic pathway:

$$\mathrm{PrP^{c}} \xrightarrow{k} \mathrm{PrP^{Sc}} \xrightarrow{\gamma} \text{PrP-amyloid}. \qquad [1]$$

We describe the mathematical model of the disease kinetics in detail in Appendix 1. The within-cell dynamics consist of the $PrP^{c} \rightarrow PrP^{Sc}$ conversion; $PrP^{Sc}$ is free to move and can infect other cells (17). Strain parameters enter the dynamics in a straightforward way: for greater values of $k$, more $PrP^{Sc}$ is produced more quickly, whereas greater values of $\gamma$ increase the rate of PrP-plaque deposition. The parameter $b_{ij}$ determines the rate of cell to cell diffusion and $\alpha/\beta$ control the rate of $PrP^{c}$ production/decay. The parameter $K$ determines the average number of connections among cells (to capture close apposition and synaptic contact). Because of computational limitations we simulate values of $K$ in series in the order of tens of connections rather than thousands.

## Results

**Effects of Varying $PrP^{c}$ Turnover.** It has been observed that increased production of $PrP^{c}$ reduces the latency of prion disease onset (18). In Fig. 1 *a* and *b* we follow the accumulation of $PrP^{c}$ in a 25 by 25 array of simulated nerve cells for different rates of $PrP^{c}$ production. Infection is initiated by inoculation of $PrP^{Sc}$ into the cell in the center of the array, assuming a baseline level of $PrP^{c}$ production (Fig. 1*a*) and a higher rate of production (Fig. 1*b*). After a short period (T2) infection has spread to a number

MICROBIOLOGY

Abbreviations: PrP, prion protein; $Prp^{Sc}$, protease-resistant isoform of PrP; $Prp^{c}$, cellular PrP; CJD, Creutzfeldt-Jakob disease; GSS, Gerstmann-Sträussler-Scheinker syndrome; FII, fatal familial insomnia.

†To whom reprint requests should be addressed.

The publication costs of this article were defrayed in part by page charge payment. This article must therefore be hereby marked "*advertisement*" in accordance with 18 U.S.C. §1734 solely to indicate this fact.

Article published online before print: *Proc. Natl. Acad. Sci. USA*, 10.1073/pnas.180317097. Article and publication date are at www.pnas.org/cgi/doi/10.1073/pnas.180317097

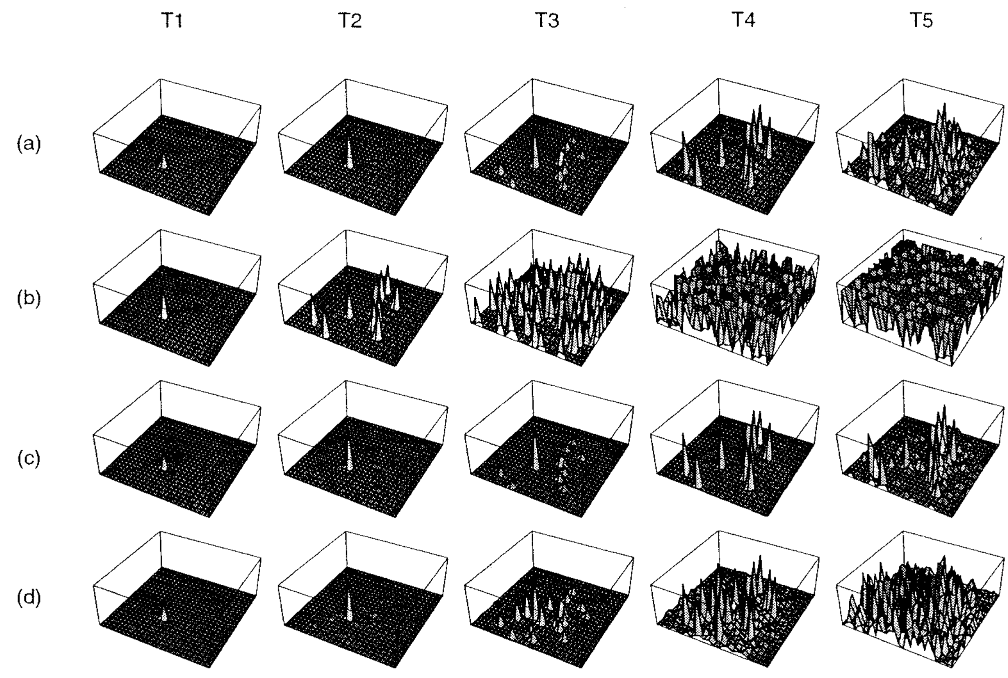


**Fig. 1.** $PrP^{Sc}$ accumulation pattern over time. (*a*) $\alpha = 200$ and no inhibition for $K = 4$. (*b*) Effect of increased $PrP^c$ production, $\alpha = 250$ (no inhibition, $K = 4$). (*c*) Effect of axonal inhibition as $PrP^{Sc}$ is accumulated ($\alpha = 250$, $K = 4$). (*d*) Effect of higher local connectivity, $K = 8$ ($\alpha = 250$, no inhibition). In all cases six long-range axons have randomly been placed between cells in addition to the $K$ local connection per neuron.

of cells through bidirectional connections in Fig. 1 *a* and *b*. In Fig. 1*a* the concentration of $PrP^{Sc}$ in each cell other than at the site of the inoculum remains negligible. By contrast, the high production series (Fig. 1*b*) shows that each of the strongly connected cells already has accumulated considerable $PrP^{Sc}$. By T3 the low turnover series (Fig. 1*a*) is building up $PrP^{Sc}$ concentration, whereas the high production series is already nearing saturation. Thus turnover significantly influences the spatial and temporal distribution of $PrP^{Sc}$.

The same pattern is true for the distribution of PrP-amyloid (Fig. 2). The high turnover series (Fig. 2*b*) shows a much faster rate of deposition and a more abundant distribution of amyloid than the baseline infection (Fig. 2*a*).

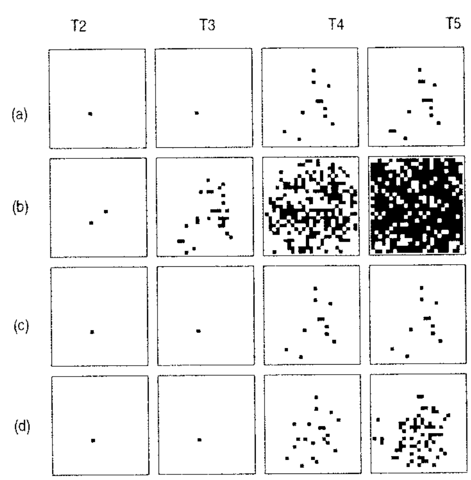


**Fig. 2.** PrP-amyloid deposition patterns for the same parameters as in Fig. 1. (*a*) $\alpha = 200$, no inhibition, $K = 4$. (*b*) Effect of increased $PrP^c$ production. (*c*) Effect of inhibition of axonal transport. (*d*) Effect of increased local connectivity.

**Inhibitory Effects of $PrP^{Sc}$.** If the strength of the interneuronal connections is weakened by $PrP^{Sc}$-induced killing of target cells, the spread of the infectious agent will be reduced when it is at high concentrations within a cell. Thus infectious propagation can depend on the concentration gradients of $PrP^{Sc}$ and the inhibitory influence of the protein on axonal/dendritic connections. We assume a simple linear relation between $PrP^{Sc}$ concentration in the cells and strength of the inter neuronal connection (see Appendix 2). In Fig. 1*c* we follow the influence of inhibition on the accumulation of $PrP^{Sc}$ through time. In the early stages of infection inhibition has little influence on the propagation of infection, because intracellular $PrP^{Sc}$ has not yet reached a concentration that induces the axons to regress. By the final epoch, the inhibition series is distinguished by a more patchy distribution of $PrP^{Sc}$ than in the absence of inhibition. The amyloid deposition series (Fig. 2*c*) reflects this pattern only very weakly and the distribution of plaques is effectively indistinguishable from the baseline case (Fig. 2*a*).

**Effects of Local Neuronal Connectivity.** Different regions in the central nervous system possess different numbers of connections per neuron. Within the cerebellum the average number of connections a neuron can form varies from a few dozen for granular cells to 150,000 for Purkinje cells. Therefore we will next investigate the influence of structural variation in different brain regions on the patterns of $PrP^{Sc}$ and amyloid deposition.

In Fig. 1*d* we have doubled the mean connectivity in our model while keeping all other parameters fixed. Early in the infectious process we notice that more cells are involved than in the baseline infection (Fig. 1*a*). By the final stages of infection $PrP^{Sc}$ is abundant in each cell. Thus PrP deposition is increased significantly in highly connected regions, and progression to clinical disease is expected to be more rapid in these regions.

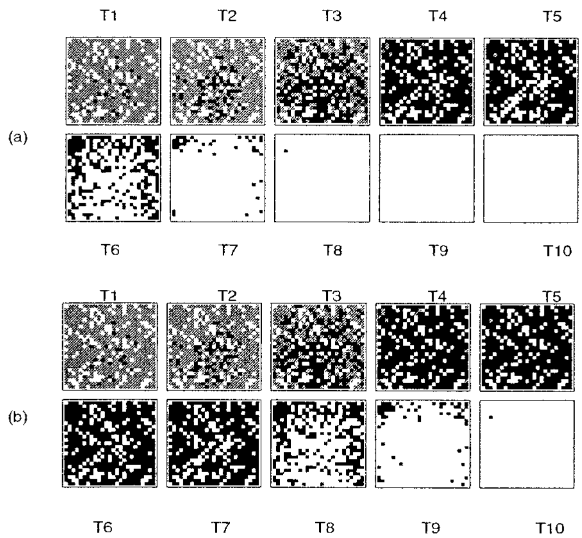


**Fig. 3.** Neurotoxicity of $PrP^{Sc}$ (*a*) vs. loss of function through $PrP^{c}$ depletion (*b*) as triggers for neuronal loss. The distribution of uninfected cells (gray), infected (black), and absence of neurons (white) for the two possible simple mechanisms are shown at 10 equidistant time intervals until all cells are dead. The arbitrary threshold was set such that the cell dies when $c(PrP^{Sc}) > 1.5 \times c_0(PrP^{c})$ (*a*) and $c(PrP^{c}) < 0.5 \times c_0(PrP^{c})$ (*b*), respectively.

Unlike high $PrP^{c}$ turnover (Fig. 2*b*) where there are many regions without amyloid-free cells, in Fig. 2*d* there are few regions in which groups of contiguous cells all have deposited plaques. In the figure this is suggested by the clusters of amyloid-free cells within infected regions.

**$PrP^{Sc}$ Accumulation Vs. $PrP^{c}$ Depletion and Neuronal Loss.** There is mounting evidence that apoptosis is responsible for cell death in prion diseases (19, 20). We explore two possible mechanisms for the induction of cell loss. In one, $PrP^{Sc}$ accumulation directly induces cell death by invoking the apoptotic pathway. In the second mechanism, $PrP^{c}$ is assumed to play a (as yet unknown) crucial role in the neuron; $PrP^{c}$ depletion therefore leads to cell death through loss of function. These two mechanisms are implemented, assuming either that (*i*) a 50% reduction of the $PrP^{c}$ concentration leads to cell death or (*ii*) a $PrP^{Sc}$ concentration exceeding the normal cellular concentration of $PrP^{c}$ in the healthy cell by 50% produces cell death.

In Fig. 3 we plot the time course of neuronal loss. In the top series (Fig. 3*a*) we assume direct activation of apoptosis whereas in the bottom series we assume death through loss of function (Fig. 3*b*). Over the first four epochs of infection degeneration is indistinguishable. This is because we are seeing the early phase of infection, during which there is transport and transformation of susceptible cells rather than cell death. By the time T5 the $PrP^{Sc}$ neurotoxicity series (Fig. 3*a*) is beginning to show signs of cell death as more of the brain degenerates. At T6 the differences between the two treatments have become very pronounced. $PrP^{Sc}$ accumulates rapidly within the infected cells in a density-dependent fashion, whereas $PrP^{c}$ depletes slowly as cells are constantly synthesizing new PrP, resulting in a delayed onset of cell loss.

The differences in PrP-amyloid deposition are more revealing. In Fig. 4 we plot the absolute amyloid concentrations for epochs T1, T5, and T10 corresponding to Fig. 3. Assuming a toxic PrP we see very little amyloid deposition as the rapid accumulation of $PrP^{Sc}$ kills cells before they can deposit large numbers of plaques. Whereas with loss of function, cells die at a lower rate and thereby allow a greater amount of amyloid to be deposited over the protracted lifetime of the cells.

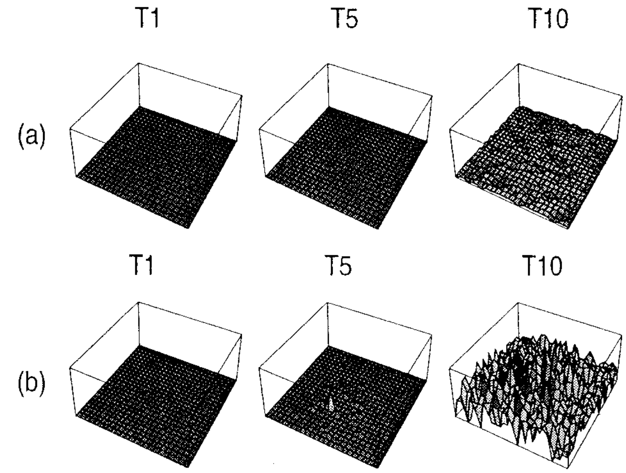


**Fig. 4.** Spatial PrP-amyloid deposition characteristics for the case of $PrP^{Sc}$ neurotoxicity (*a*) and $PrP^{c}$ depletion (*b*) as triggers for neuronal loss. The time labels refer to the corresponding times in Fig. 3. Depletion results in significantly higher (by a factor of $\approx$10) concentrations of PrP-amyloid than neurotoxicity.



**Effects of Cellular Tropism.** Tropism of $PrP^{Sc}$ for different neuronal cell types has been proposed as an explanation for the diversity of prion-associated pathologies upon infection with different $PrP^{Sc}$ strains (21, 22). We model tropism as strain-specific rates $k$ of transformational change of $PrP^{c}$ into $PrP^{Sc}$. Thus a strain has a higher rate of transformation within cells for which it has a preferential tropism.

In Fig. 5*a* we have assumed that $k = k_0$ in the front half of the lattice and $k = 2 \times k_0$ in the back half ($k_0 = 0.0001$). In Fig. 5*b* we have moved the site of initial inoculation. Independent of the site of inoculation, $PrP^{Sc}$ deposition and disease progression are

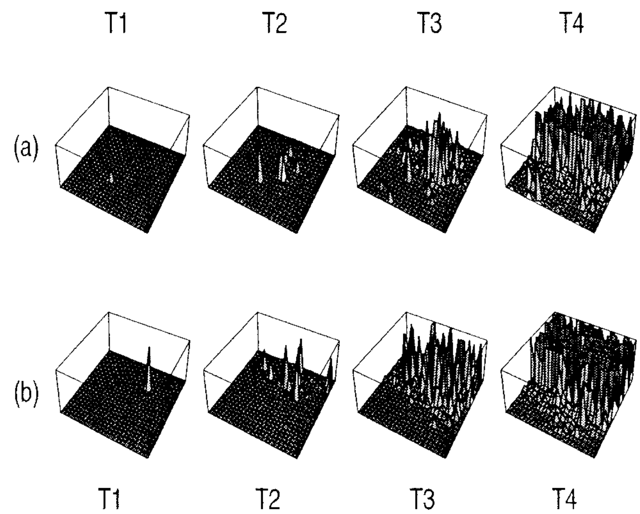


**Fig. 5.** Neurotropism as a cause for characteristic $PrP^{Sc}$ accumulation patterns. In our model neurotropism is attributed to a local difference in the $PrP^{Sc}$ replication rate, $k$. The initial infection sites are clearly visible in the T1 frames. Because of the higher value of $k$ in the neurons in the rear part of the spatial model, $PrP^{Sc}$ deposition is increased in that region whereas comparatively little $PrP^{Sc}$ accumulates in the front half.

more pronounced in the region with the higher value of $k$. If different forms of $PrP^c$ do occur in the same brain, then it is possible for small variations in the value of $k$ associated with different strains to lead to radically different $PrP^{Sc}$ accumulation patterns.

## Discussion

We have modeled neuropathogenesis by a spatial model incorporating the reaction kinetics of $PrP^c$ conversion to $PrP^{Sc}$. Using the modeling approach we have attempted to separate out strain- and host-dependent factors. In the following qualitative discussion we relate our results to empirical findings. We were only able to show characteristic cases but our study has shown remarkable robustness in all of the parameters including $k$, $\gamma$, and $K$. Moreover we found that the results for the cell loss triggers are qualitatively the same for a wide range of threshold values. Simulations were run with up to 5,000 cells, and no qualitative difference was found for the smaller numbers presented here. The documented C-source code used for the simulations can be downloaded on our web site: http://mathbiol.zoo.ox.ac.uk/michael/prions.html.

The model shows the huge influence $PrP^c$ turnover and neuronal connectivity exerts on disease progression. Axonal regression, which is observed in prion diseases (23), on the other hand, was not found to alter the spatial dynamics of the infectious agent significantly. Loss of connectivity is, however, functionally equivalent to loss of neurons, and we therefore expect to find neurological change as axons regress.

The model shows that neuronal connectivity profoundly influences pathogenesis; it is probably the high density of neuronal connections in the cerebellum (which holds about 30% of the neurons in 10% of the total volume of the brain) that gives rise to the very similar early clinical progressions observed in the human prion diseases. This is also confirmed by neuropathology: in kuru and GSS PrP-amyloid is found at relatively high concentrations in the cerebellum. Neuronal loss is also most severe in GSS (3–5).

As a result of the use of mice overexpressing PrP in experimental inoculation studies (9, 24) pathology often differs from naturally occurring diseases (where oral intake is presumably more common). $PrP^c$ overexpression accelerates intracellular replication dynamics and loss of neurons. This has the result that early clinical symptoms stem from neuronal degradation close to the inoculation site and not from damage to regions toward which $PrP^{Sc}$ is "naturally" attracted. To gain a better understanding of human prion disease pathogenesis it therefore seems important to use transgenic models that (*i*) are inoculated orally and (*ii*) do not overexpress human $PrP^c$. The problem is that overexpression is required to ensure infection over a manageable time scale; but, using the modeling approach outlined above, predictions about the pathology in naturally occurring disease also can be derived from experiments with overexpressing mice.

Although the precise mechanism by which neuro-degeneration occurs remains uncertain, evidence suggests that apoptosis is responsible for neuronal death (19, 20). The accumulation of $PrP^{Sc}$ could induce neurons to enter into apoptosis either through direct activation of cell death (25, 26) or through the competitive elimination of essential $PrP^c$ molecules (27). The former explanation often has been favored as prion knockout mice exhibit few deleterious phenotypes (40). In the absence of positive, conditional knockout mice models the nature of the cell loss trigger remains currently undecided by experiments (2).

Our model has allowed us to explore the neuropathological implications of both of these mechanisms. In the case where $PrP^{Sc}$ is neurotoxic, a large number of cells are induced into cell death before an appreciable quantity of PrP-amyloid has been deposited. Whereas when cell death results from $PrP^c$ depletion, cells take a longer time to die and thereby produce a much larger quantity of PrP-amyloid. Thus abundant PrP-amyloid may be symptomatic of loss of function, whereas cell loss may be symptomatic of direct activation of apoptosis. With this result in mind we can contrast the pathologies of CJD, GSS, and FFI. In CJD there is a large amount of cell death and relatively few plaques. In GSS (and also in kuru) there are numerous plaques and less cell death. We hypothesize that in CJD and in particular in FFI, $PrP^{Sc}$ is able to directly induce cell loss. By contrast, $PrP^{Sc/GSS}$ is less toxic and hence cell death is primarily a consequence of $PrP^c$ depletion. Of course, amyloid frequency also reflects the strain and potentially the body's capability of partially digesting that particular strain.

Numerous studies have demonstrated that $PrP^{Sc}$ accumulation is highly strain-dependent (22). The existence of differentially glycosylated $PrP^c$ forms in the same host brain or of different molecular chaperones in the $PrP^c \rightarrow PrP^{Sc}$ structural change can lead to radically different $PrP^{Sc}$ and PrP-amyloid accumulation patterns and lesion profiles. A recent finding is that in scrapie-infected mice, cortical parvalbumin neurons are severely reduced whereas calbindin and calretinin neurons remain unaffected (29). In CJD-inoculated mice, loss of parvalbumin neurons is severe and occurs very early after inoculation (30).

Although we cannot explain the mechanisms behind cellular tropism of $PrP^{Sc}$ with our model, we can approximate them, assuming differences in the replication rate of $PrP^{Sc}$ with different forms of $PrP^c$. Thus an important result of our model has been to show how partial tropism can lead to strain-specific $PrP^{Sc}$ accumulation patterns. In fact, at least in our model, in a protein-only mechanism of transmissible spongiform encephalopathies cellular tropism is both necessary and sufficient to generate different pathological phenotypes.

The present work suggests a path toward an understanding of prion-related pathogenesis. We believe that by adding structural detail to the model predictions for empirically derived $PrP^{Sc}$ accumulation patterns after inoculation are in reach. Furthermore, the model provides a conceptual assay of the neurotoxicity of different $PrP^{Sc}$ isoforms in prion diseases.

## Appendix 1: The Kinetic Model

We model prion propagation with the following system of ordinary differential equations:

$$\dot{x}_i(t) = \alpha_i - kx_i(t)y_i(t) - \beta_i x_i(t), \quad [2]$$

$$\dot{y}_i(t) = kx_i(t)y_i(t) - \sum_{j=1}^{N} (b_{ij}y_i(t) - b_{ji}y_j(t)) - \gamma y_i(t), \quad [3]$$

$$\dot{z}_i(t) = \gamma y_i(t), \quad [4]$$

where $x$, $y$, $z$ represent the concentrations of $PrP^c$, $PrP^{Sc}$, and extracellular PrP plaques, respectively, and the index $i$ labels the cells. $PrP^c$ is assumed to be created at a cell specific rate $\alpha_i$ and destroyed within cells at a rate $\beta_i$ (in the absence of tropism we have $\alpha_i = \alpha$ and $\beta_i = \beta\ \forall i$). $PrP^c$ is converted into $PrP^{Sc}$ upon contact at a rate $kx_i(t)y_i(t)$ (15). We assume that $PrP^{Sc}$ spreads predominantly along axons and dendrites by slow axonal transport (17). The rate of $PrP^{Sc}$ spread from one cell to another is a function of the connection strength, $b_{ji}$, and the difference in concentration of the diffusing $PrP^{Sc}$, $|y_i(t) - y_j(t)|$. Because $PrP^c$ is uniformly distributed throughout the mammalian brain we believe that $PrP^c$ diffusion is negligible. Assuming symmetrical transport we have for the elements of the connectivity matrix ($b_{ij}$)

$$b_{ij} = \frac{b}{d_{ij}}\mu_{ij} \quad \text{with} \quad d_{ij} = |\mathbf{r}_i - \mathbf{r}_j|. \quad [5]$$

The parameter $d_{ij}$ is the metric distance between cells $i$ and $j$; $\mu_{ij}$ embodies the local structure of the brain and is defined by

$$\mu_{ij} = \begin{cases} 1 & \text{if } i, j \text{ are connected by a neuronal process} \\ 0 & \text{otherwise.} \end{cases} \quad [6]$$

The PrP bound in plaques, $z$, remains attached to the cell where it is produced, thereby assuming negligible rates of transport of (amyloid) plaques.

The cellular dynamics of the $PrP^c/PrP^{Sc}$ system (Eqs. **2** and **3**) show two equilibria,

$$x_i = \frac{\alpha_i}{\beta_i}, y_i = 0, \quad [7]$$

$$x_i = \frac{\gamma}{k}, y_i = \frac{\alpha_i}{\gamma} - \frac{\beta}{k}. \quad [8]$$

Eq. **7** represents the case of no infection where the $PrP^c$ abundance is determined by the ratio of its production and decay rates. Eq. **8** is the infection equilibrium and hence the $PrP^c$ abundance is given by the ratio of transformation rate and $PrP^{Sc}$ decay rate. It is important to note that $PrP^{Sc} >> PrP^c$ at the infectious equilibrium. The equilibria do not depend on the connective strengths among cells ($b_{ij}$).

## Appendix 2: Axonal Regression

We define the function whereby axons and dendrites degenerate according to the death of anterograde and retrograde nerve cells. Assuming that the cells provide connections with some form of trophic support we write

$$\bar{b}_{ij} = \frac{(y_0 - y_i)(y_0 - y_j) \times \Theta(y_0 - y_i)\Theta(y_0 - y_j)}{{y_0}^2}. \quad [9]$$

Here $y_0$ is the threshold level of $PrP^{Sc}$ at which the connection breaks down and $y_i$, $y_j$ are the concentrations of $PrP^{Sc}$ in cells $i$ and $j$. The step functions [$\Theta(y_0 - y_{i/j})$ $\Theta(X) = 0$ for $x < 0$ and $\Theta(x) = 1$ for $x > 0$] ensure that ($i$) the axon "dies" if the $PrP^{Sc}$ concentration exceeds the critical level $y_0$ and ($ii$) 1 $\bar{b}_{ij} \geq 0$. Eq. **9** is the simplest representation of a function describing inhibition of axonal transport with increased $PrP^{Sc}$ deposition, and we can multiply the right-hand side of Eq. **5** by $\bar{b}_{ij}$ to arrive at a inhibitory connectivity matrix. In general we expect that the axons regress before the neurons die, i.e., $y_0 < y_c$.

We thank Lynn Enquist for his insightful comments on the manuscript. M.P.H.S. gratefully acknowledges support through fellowships from the Wellcome Trust and Linacre College, Oxford. D.C.K. thanks the Leon Levy and Shelby White Initiatives Fund, the Florence Gould Foundation, the J. Seward Johnson, Sr. Charitable Trusts, the Ambrose Monell Foundation, and the Alfred P. Sloan Foundation.

1. Prusiner, S. (1982) *Science* **216,** 136–144.
2. Aguzzi, A. & Weissmann, C. (1997) *Nature (London)* **389,** 795–798.
3. Bell, J. & Ironside, J. (1993) *Br. Med. Bull* **49,** 738–777.
4. Ironside, J. & Bell, J. (1997) in *Prion Diseases*, eds. Collinge, J. & Palmer, M. (Oxford Univ. Press, Oxford), pp. 57–88.
5. DeArmond, S. & Ironside, J. (1999) in *Prion Biology and Diseases*, ed. Prusiner, S. (Cold Spring Harbor Lab. Press, Plainview, NY), 585–652.
6. Bruce, M. (1993) *Br. Med. Bull.* **49,** 822–838.
7. Lasmezas, C., Deslys, J., Demaimay, R., Adjou, K., Hauw, J. & Dormont, D. (1996) *J. Gen. Virol.* **77,** 1601–1609.
8. Prusiner, S., Fuzi, M., Scott, M., Serban, D., Serban, H., Taraboulos, A., Gabriel, J., Wells, G., Wilesmith, J., Bradley, R., *et al*. (1993) *J. Infect. Dis* **167,** 602–613.
9. DeArmond, S. & Prusiner, S. (1995) *Brain Pathol.* **5,** 77–89.
10. Bradley, R. (1997) in *Prion Diseases*, eds. Collinge, J. & Palmer, M. (Oxford Univ. Press, Oxford), pp. 89–129.
11. Parchi, P., Giese, A., Capellari, S., Brown, P., Schulz-Schaeffer, W., Windl, O., Zerr, L., Budka, H., Kopp, N., Piccardo, P., *et al*. (1999) *Ann. Neurol.* **46,** 224–233.
12. Griffiths, J. (1967) *Nature (London)* **215,** 1043–1044.
13. Eigen, M. (1996) *Biophys. Chem.* **63,** A1–A18.
14. Payne, R. & Krakauer, D. (1998) *Proc. R. Soc. London Ser. B* **265,** 2341–2346.
15. Nowak, M., Krakauer, D., Klug, A. & May, R. (1998) *Integrative Biol.* **1,** 3–15.
16. Masel, J., Jansen, V. & Nowak, M. (1999) *Biophys. Chem.* **77,** 139–152.
17. Scott, J. & Fraser, H. (1989) *Brain Res.* **504,** 301–305.
18. Prusiner, S., Groth, D., Serban, A., Koehler, R., Foster, D., Torchia, M., Burton, D., Yand, S. & DeArmond, S. (1993) *Proc. Natl. Acad. Sci. USA* **90,** 10608–10612.
19. Giese, A., Groschup, M., Hess, B. & Kretzschmar, H. (1995) *Brain Pathol.* **5,** 213–221.
20. Schatzl, H., Laszlo, L., Holtzman, D., Tzelt, J., DeArmond, S., Weiner, R., Mobley, W. & Prusiner, S. (1997) *J. Virol.* **71,** 8821–8831.
21. DeArmond, S., Yang, S., Cayetano-Canlas, J., Groth, D. & Prusiner, S. (1994) *Philos. Trans. R. Soc. London B* **343,** 415–423.
22. DeArmond, S., Sanchez, H., Yehiely, F., Qiu, Y., Ninchak-Casey, A., Daggett, V., Camerino, A., Cayetano, J., Rogers, M., Groth, D., *et al*. (1997) *Neuron* **19,** 1337–1348.
23. Clinton, J., Forsyth, C., Royston, M. & Roberts, G. (1993) *NeuroReport* **4,** 65–68.
24. Raeber, A., Brander, S., Klein, M., Benninger, Y., Musahl, C., Frigg, R., Roeckl, C., Fischer, M., Weissmann, C. & Aguzzi, A. (1998) *Brain Pathol.* **8,** 715–733.
25. Lin, M., Mirzabekov, T. & Kagan, B. (1997) *J. Biol. Chem.* **272,** 44–47.
26. Florio, T., Thellung, S., Amico, C., Robello, M., Salmona, M., Bugiani, O., Tagliavini, F., Forloni, G. & Schettini, G. (1998) *J. Neurosci. Res.* **54,** 341–352.
27. Kuwahara, C., Takeuchi, A., Nishimura, T., Haraguchi, K., Kubosaki, A., Matsumoto, Y., Sacki, K., Matsumoto, Y., Yokoyama, T., Itohara, S., *et al*. (1999) *Nature (London)* **400,** 225–226.
28. Katamine, S., Nishida, N., Sugimoto, T., Noda, T., Sakaguchi, S., Shigematsu, K., Kataoka, Y., Hasegawa, S., Moriuchi, R. & Miyamoto, T. (1998) *Cell. Mol. Neurobiol.* **18,** 731–742.
29. Yun, S., Choi, E., Ju, W., Ahn, M., Carp, R., Wisniewski, H. & Kim, Y. (1998) *Mol. Chem. Neuropathol.* **34,** 121–132.
30. Guentchev, M., Groschup, M., Kordek, R., Liberski, P. & Budka, H. (1998) *Brain Pathol.* **8,** 615–623.